Electronic Supplementary Information (ESI)

Solvent-free synthesis, coating and morphogenesis of conductive polymer materials through spontaneous generation of the activated monomers

Ryo Muramatsu,[a] Yuya Oaki, [a]* Kento Kuwabara, [a] Kosei Hayashi, [b] Hiroaki Imai [a]*

[a]Department of Applied Chemistry, Faculty of Science and Technology, Keio University, 3-14-1 Hiyoshi, Kohoku-ku, Yokohama 223-8522, Japan

[b]Tokyo Metropolitan Industrial Technology Research Institute, 2-4-10 Aomi, Koto-ku, Tokyo 135-0064, Japan

*E-mail: oakiyuya@applc.keio.ac.jp (Y. O.), hiroaki@applc.keio.ac.jp (H. I.)

Contents

Experimental Methods

Polymerization of the Heteroaromatic Compounds. All the reagents were used as purchased without further purification. The typical experimental setup was illustrated in Fig. 1a. A small glass bottle typically 6 cm^3 containing 0.24 g of $Cu(NO_3)_2 \cdot 3H_2O$ (Kanto, 99.0 %) or $Fe(NO_3)_3 \cdot 9H_2O$ (Kanto, 99.0 %) was put in a large outer glass vessel typically 40 cm^3 containing 1.0 cm^3 of heteroaromatic monomers, such as pyrrole (Py, Kanto, 99.0%), 3,4-ethylenedioxythiophene (EDOT, TCI, 98.0%), 3-hexylthiophene (3HT, TCI, 98.0%), and thiophene (Tp, Kanto, 98.0%). The following substrates were attached on the cap of the vessel; the cleaned glass slide, single crystal blocks ca. 5 mm in size of potassium bromide (KBr), potassium chloride (KCl), and calcite-type calcium carbonate ($CaCO_3$), and silicon (Si) wafer. In another setup, the two small glass bottles containing the monomers and the oxidant crystals were put in the large glass vessel. The substrates were set at the bottom of the outer glass vessel. In any cases, the outer sample bottle was closed by a screw cap with a thin Teflon tape. After the sealing, the sample bottle was placed in an incubator at 60 ˚C for 0.5 h to 120 h. After the reaction, the substrates were maintained and dried to remove the unremoved monomers at 60 ˚C. In the other setup, the two small sample bottles containing the monomers and the oxidant crystals were set in the outer sample bottle. The substrates were put in the bottom of the outer sample bottle.

PPy Coating on a Sea Urchin Spine. The spines of a sea urchin (*Echinometra mathaei*), a model of complex hierarchical morphology, were immersed in 5 wt.-% sodium hypochlorate (NaClO) aqueous solution for 24 h to remove the incorporated biological macromolecules. The same treatment was performed in the fresh NaClO aqueous solution, again. After the washing by purified water, the sea urchin spines were treated at 450°C for 12 h in air to expand the nanospace for the incorporation of the monomer vapor. The spine of a sea urchin was set in the sample bottle as the substrate. PPy was deposited on a sea urchin spine. After the polymerization at 60 ˚C for 60 h by using $Fe(NO_3)_2 \cdot 9H_2O$, the resultant material was collected. The exoskeleton of a sea urchin spine consisting of calcium carbonate was dissolved with immersion in 0.1 mol dm^{-3} hydrochloric acid (HCl) for 24 h. After the washing by purified water, the PPy architecture was obtained by freeze-drying.

PPy Coating of Lithium Titanate Nanocrystals. A commercial lithium titanate nanocrystal ($Li_4Ti_5O_{12}$, Aldrich, 99%) less than 100 nm in the size was used as the substrates in the sample bottle for the polymerization. The polymerization was performed at 60 ˚C for 3 h by using $Fe(NO_3)_2 \cdot 9H_2O$. The resultant PPy/$Li_4Ti_5O_{12}$ composite was used for the active material of lithium ion battery. The electrochemical measurement was performed by using a three electrode setup in a twin-beaker cell. The working electrodes were prepared by mixing of 70 wt.-% active materials, 20 wt.-% acetylene black carbon, and 10 wt.-% PTFE binder. The

working electrode was pressed onto a nickel mesh (Nilaco, 200 mesh). The counter and reference electrodes were composed of lithium metal. The electrolyte was 1 mol dm^{-3} $LiClO_4$ in ethylene carbonate (EC) and diethylene carbonate (DEC) (1/1 by volume).

Characterization. The morphologies of the resultant materials were observed by optical microscopy (Keyence VE-1000 and Olympus BX81-FL), field-emission scanning electron microscopy (FESEM, FEI Sirion and Hitachi S-4700 operated at 5.0 kV), and field-emission transmission electron microscopy (FETEM, FEI Tecnai F20 operated at 200 kV). For FETEM observation, the polymer films were obtained by the dissolution of the KBr substrates with purified water. The dispersion liquid of the resultant films was dropped on a collodion membrane supported by a copper grid. The remaining metal components were analyzed by energy-dispersive X-ray spectroscopy (EDX, Bruker Quantax) on the FESEM observation. The crystal structures of the oxidant crystals were analyzed by X-ray diffraction (XRD, Rigaku Mini Flex II and Bruker D8 Advance with CuKα radiation). The structures of the polymers were characterized by Fourier-transform infrared (FT-IR) absorption spectroscopy (JASCO, FT/IR-4200) and CHN elemental analysis. The vapor in the sample bottle was analyzed by gas chromatograph mass spectroscopy (GC-MS, Agilent 7890A GC system combined with Agilent 5975C inert XLMSD). The vapor generated in the sample bottle at 60 ˚C was directly injected in the column of GC-MS at 60 ˚C. The cmount of PPy coated on the $Li_4Ti_5O_{12}$ nanocrystals was analyzed under air atomsphere by thermogravimetric (TG) analysis (SII, TG/DTA 7200).

Influence of the substrates and the other oxidative agents

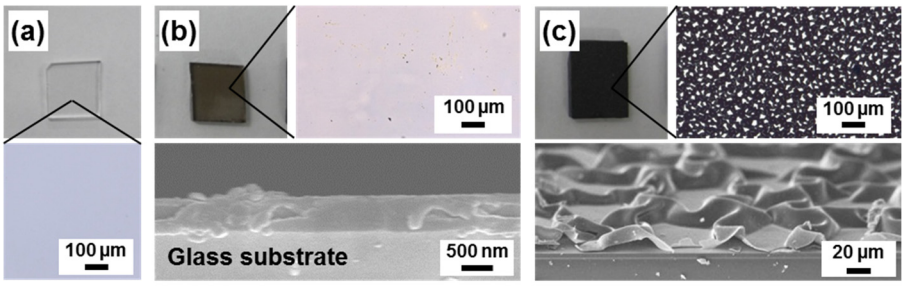

Fig. S1. Polymerization and coating of PPy on a glass substrate in the presence of $Cu(NO_3)_2 \cdot 3H_2O$. (a) a glass substrate before polymerization. (b,c) the surface views by OM (upper panels) and the cross-sectional images by FESEM (bottom panels) of PPy deposited on a glass substrate for 3 h (b) and 60 h (c).

The flat and wrinkled films of PPy were obtained on a glass substrate. The morphology of the wrinkled films was different from that formed on a KBr substrate, as shown in Fig. 1f,g. The patterned morphologies consisting of the wrinkled films depended on the sorts of the substrates (Fig. S2 in the ESI).

The oxidative agent was changed to the other copper salts and the nitrates. Although the color of the crystal surfaces was changed on the copper sulfate pentahydrate ($CuSO_4 \cdot 5H_2O$) and copper acetate monohydrate ($Cu(CH_3COO)_2 \cdot H_2O$), the coating was not achieved on the substrates. No color changes on the crystal surfaces and sample bottles were observed in the presence of barium nitrate ($BaNO_3$) and calcium nitrate tetrahydrate ($CaNO_3 \cdot 4H_2O$). These results suggest that the nitrate and chloride salts of the reducible metal ions mediate the polymerization and coating not only on the crystal surfaces but also on substrates in the sample bottles.

The difference of the deposition rates, as shown in Figure 2, is ascribed to the reducing character of the metal ions and the stability of the reduced species.

Morphology variation of the wrinkled films

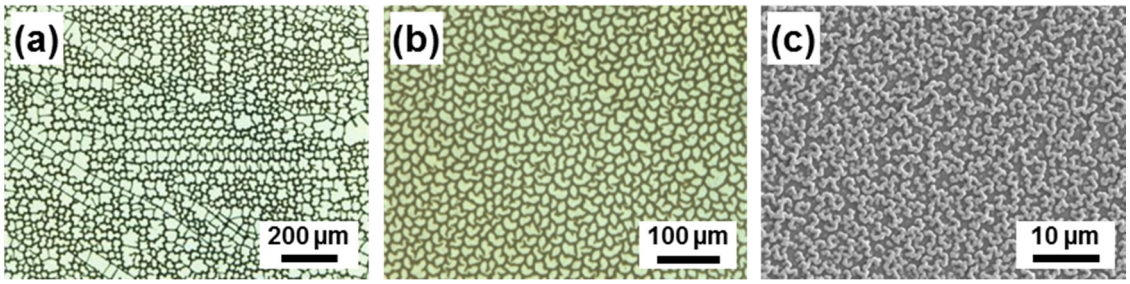

Fig. S2. Optical microscopy (a,b) and FESEM images (c) of the wrinkled films formed on the (001) face of potassium chloride (KCl) single crystal (a), the (001) face of silicon (Si), and the (104) face of calcite calcium carbonate (c).

The wrinkled films showed the morphological variety depending on the sorts of the substrates. While the flat films were obtained on the substrates in the early stage, the formation of the wrinkled films was observed in the later stage. The flat films consisted of the nanoparticles (Fig. S3). The growth of nanoparticles proceeds with an increase in the reaction time. After the formation of the dense film, the further growth of the nanoparticles induces the internal stress in the film. Therefore, the wrinkled films were formed on the substrates. Since the interaction between the polymer films and the substrates are different, the morphological variety of the wrinkled films is observed (Fig. S2).

Time-course observation of PPy formed on a substrate

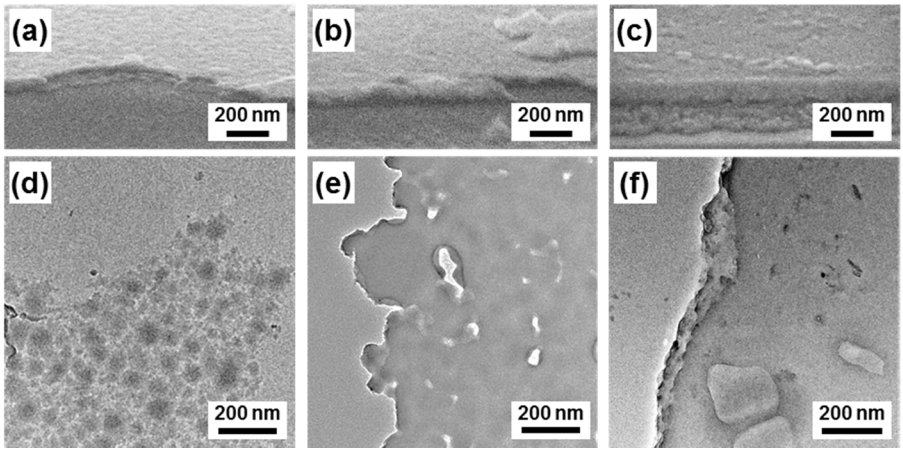

Fig. S3. Cross-sectional FESEM (a–c) and the FETEM images (d–f) of the PPy after the reaction for 0.5 h (a,d), 1 h (b,e), and 3 h (c,f).

Formation of PEDOT films

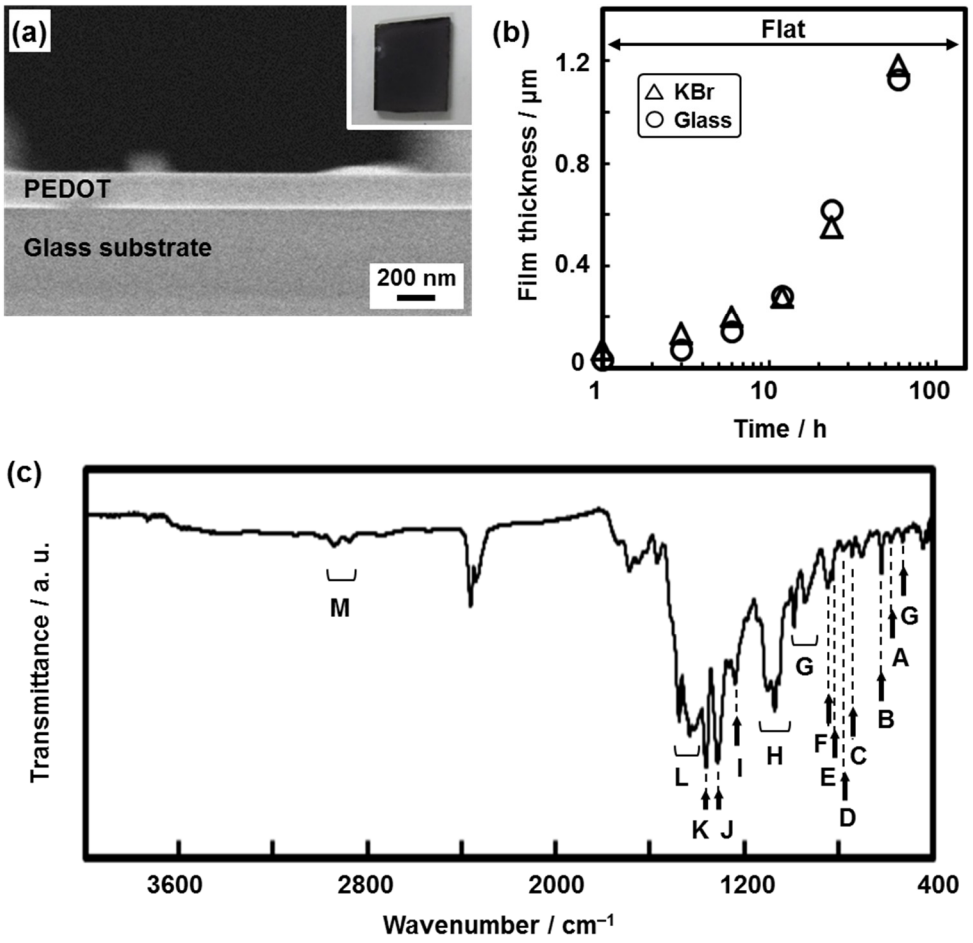

Fig. S4. Synthesis and coating of the PEDOT films on a KBr single crystal. (a) FESEM images with the macroscopic views (insets). (b) the relationship between the deposition time and the film thickness. (c) FT-IR spectra. The peaks of FT-IR spectra are assigned to the following vibrations of PEDOT: C–O–C deformation in the oxyethylene ring (A), C–S–C deformation in the thiophene ring (B), CH_2 rocking (C), the oxyethylene ring deformation and bending respectively (D, E), the O–C–C deformation (F), the unidentified peaks but appeared in the reference (G), C–O stretching and C–C stretching (H), C–O–C stretching (I), N–O stretching of the nitro groups introduced in the thiophene rings (J), CH_2 bending in the oxyethylene ring (K), C=C stretching in the thiophene ring (L), CH_2 stretching in the oxyethylene ring (M). These peak positions were consistent with the previous works.[R1]

The PEDOT films were obtained by the changes of the monomer from Py to EDOT. The flat film of PEDOT 200 nm in thickness was formed on a glass substrate in the presence of $Fe(NO_3)_2 \cdot 9H_2O$ for 6 h (Fig. S4a). The thickness of the PEDOT films was controlled by the

reaction time (Fig. S4b). The wrinkled films were not observed on these polymers.

Reference

R1. F. Tran-Van, S. Garreau, G. Louarn, G. Froyer, C. Chevrot, *J. Mater. Chem.* **2001**, *11*, 1378.

GC-MS analysis of the vapors in the sample bottle

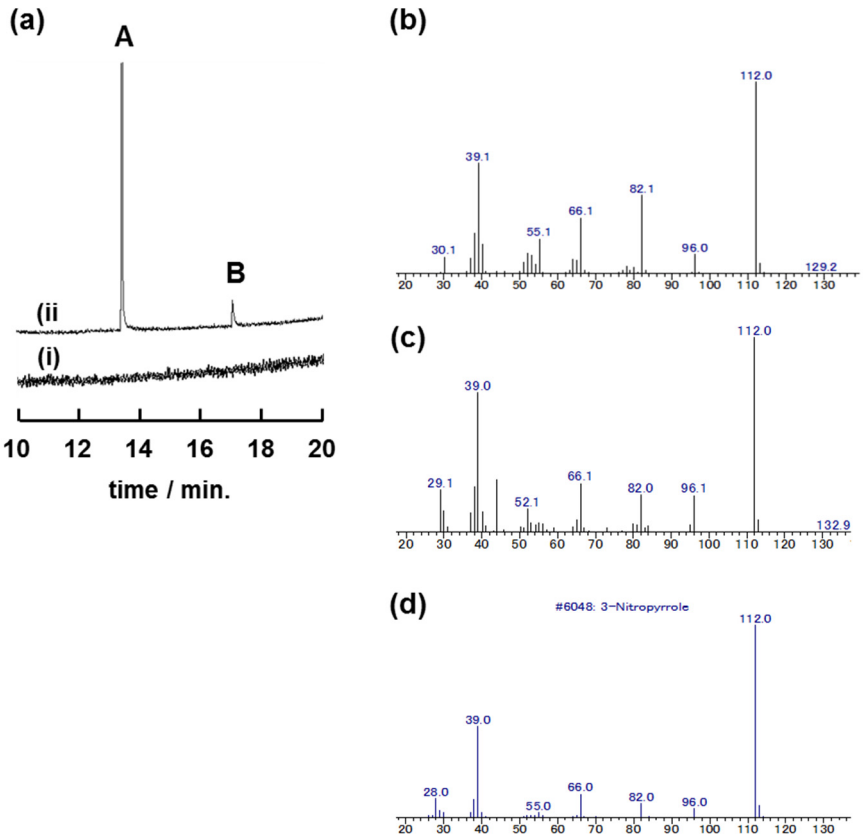

Fig. S5. GC-MS analyses of the vapors in the reaction vessel. (a) GC chart obtained at 0 h (i) and 22 h (ii). (b,c) MS chart obtained from the peaks A and B in the GC chart respectively. (d) MS chart of 3-nitropyrrole in the database.

In the MS charts, these two components were assigned to the same compound, namely nitropyrrole. These results imply that the vapors of 2-nitropyrrole and 3-nitropyrrole were formed in the sample bottle.

A proposed mechanisms for formation of PPy

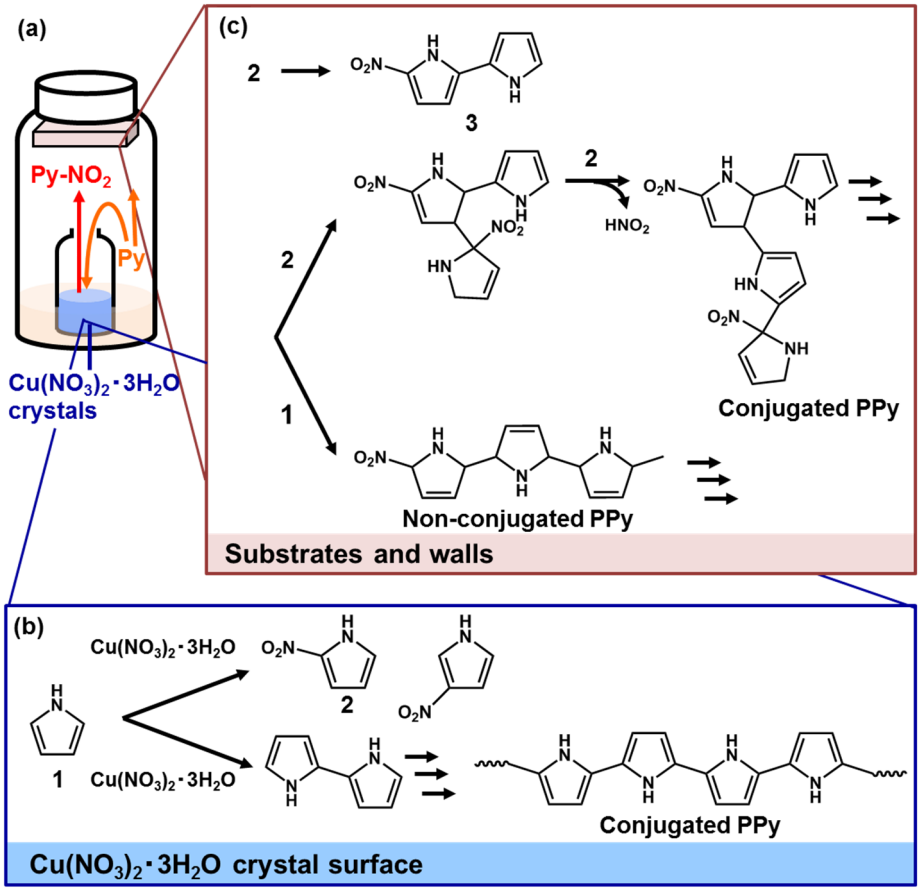

Fig. S6. Schematic illustrations for the proposed polymerization mechanisms. (a) schematic image of the sample bottle filled with the Py and Py-NO_2 vapors. (b) synthetic routes of the nitropyrolles (upper) and conjugated PPy on the surface of the $Cu(NO_3)_2 \cdot 3H_2O$ crystals (lower). The nitration and the oxidative polymerization of Py proceed. (c) synthetic routes of the conjugated and non-conjugated PPy on the substrates and walls. Both the conjugated and non-conjugated types are obtained on substrates.

In the vapor phase, the presence of pyrrole (Py) monomer and nitropyrrole (Py-NO_2) was detected by gas chromatograph mass spectroscopy (GC-MS) (Fig. S5 in the ESI). The CHN atomic ratio was estimated to be C, 4.00; H, 3.34; N, 1.27 by the elemental analysis, while the calculated value is C, 4.00; H, 3.00; N, 1.00 in the molecular structure of PPy ($(C_4H_3N)_n$). The excess amount of N is ascribed to the introduction of nitro groups in the resultant PPy. The excess amount of H implies the inclusion of the non-conjugated PPy ($(C_4H_5N)_n$) units. The non-conjugated C_4H_5N units are partially introduced in the chains of the conjugated PPy.

Therefore, the resultant PPy film showed the low conductivity, namely 4.0×10^{-5} S cm^{-1} even after iodide (I_2) doping. The reduction treatment is required for the formation of the fully-conjugated structure with the improved conductivity.

The possible polymerization mechanisms are summarized in Fig. S6. The oxidative polymerization of Py (**1**) is started on the crystal surface (Fig. S6b). When **1** is oxidized on the crystal surface, the reduction of copper ions and the elimination of the nitrate proceed. The conjugated PPy is formed by the oxidative polymerization. Along with the polymerization reaction, the nitration of **1** on the crystal surface provides 2-nitropyrrole (**2**) as the major product and 3-nitropyrrole as the minor product. The vapors of **1** and **2** diffuse in the sample bottle. The adsorption of these monomeric species initiates the polymerization on the substrates (Fig. S6c). The electron density of the pyrrole ring in **2** is lowered by the introduction of the nitro group as an electron withdrawing group. Since the nucleophilic attack of **1** to **2** leads to the coupling, the dimerized structure, namely 5-nitro-2,2'-bipyrrole (**3**), is formed.[R2–R4] Based on the same scheme, the nucleophilic attack of **1** to **3** eventually provides the non-conjugated PPy. At the same time, the electrophilic attack of **2** to **3** leads to the coupling of the Py rings. Then, the conjugated PPy is synthesized by the elimination of the nitro group as nitrous acid (HNO_2).[13] In this way, the conjugated PPy containing the non-conjugated part is formed on the substrates. The synthesis and coating of PEDOT are ascribed to the similar schemes.

The polymer films of poly(3-hexylthiophene) (P3HT) and polythiophene (PTp) were not formed on the substrates by the present approach. In general, thiophene ring is the more stable than pyrrole ring because of the resonance stabilization. It is inferred that the nitrated thiophene derivatives are not so easily formed by the electrophilic reaction. Therefore, the deposition of the P3HT and PTp films was not observed on the substrates.

Reference

R2 H. A. Porrs, G. F. Smith, *J. Chem. Soc.* **1957**, 4018.

R3 S. Sadki, P. Schottland, N. Brodie, G. Sabouraud, *Chem. Soc. Rev.* **2000**, *29*, 283.

R4 J. P. Loek, S. G. Im, K. K. Gleason, *Macromolecules* **2006**, *39*, 5326.

XRD patterns of $Cu(NO_3)_2 \cdot 3H_2O$ crystals with the polymerization

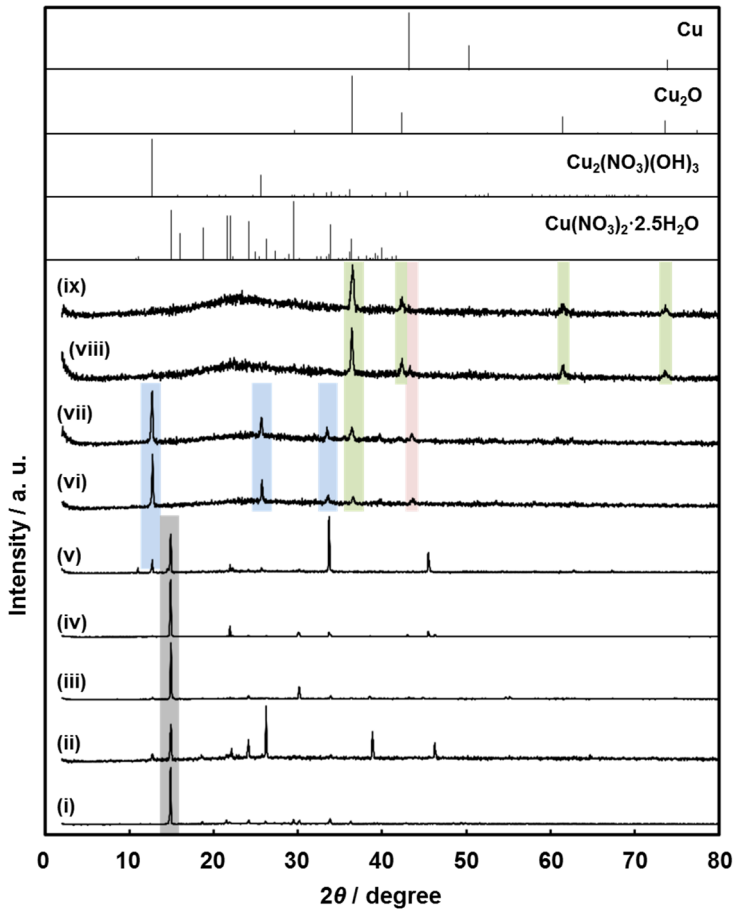

Fig. S7. Changes of the XRD patterns of the copper-related compounds with an increase in the polymerization time: (i) 0 h, (ii) 0.5 h, (iii) 1 h, (iv) 3 h, (v) 6 h, (vi) 12 h, (vii) 24 h, (viii) 60 h, (ix) 120 h.

The XRD patterns indicate that the initial $Cu(NO_3)_2 \cdot 3H_2O$ (gray marker) was gradually changed to copper nitrate hydroxide ($Cu_2(NO)_3(OH)_2$) (blue marker), copper oxide (Cu_2O) (green marker), and metallic copper (Cu) (red marker) with an increase in the deposition time. The reduction of copper ions and the elimination of nitrate ions simultaneously proceed with the polymerization.

EDX spectrum of the resultant PPy films

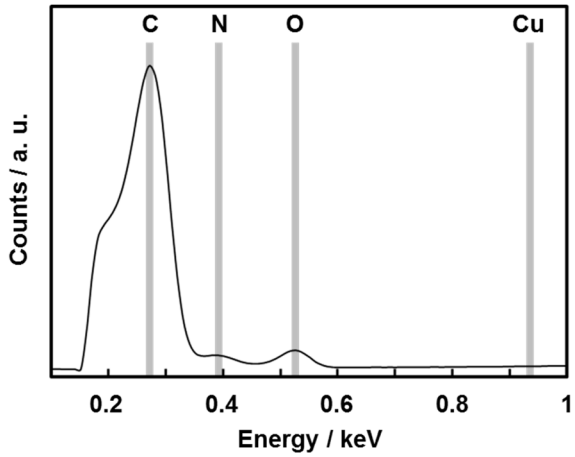

Fig. S8. EDX spectrum of the resultant PPy films.

The copper-related compounds were not contained in the resultant PPy films.

Composite of calcite and PPy formed in the replication process

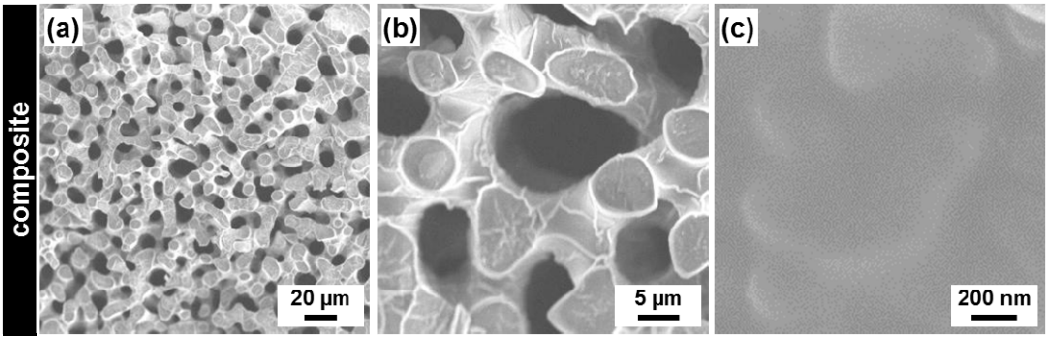

Fig. S9. FESEM images of the composite state after the polymerization.

These FESEM images show that the pores in the sponge structure were not filled with PPy. The formation and growth of PPy nanoparticles, as shown in Fig. S2, proceed in the interspace of the nanocrystals with diffusion and adsorption of the monomers. The nanospace is eventually filled with the resultant PPy. The replication scheme is similar to that by the solution processes in our previous study.[8]

PPy contents and coating behavior on the $Li_4Ti_5O_{12}$/PPy composite

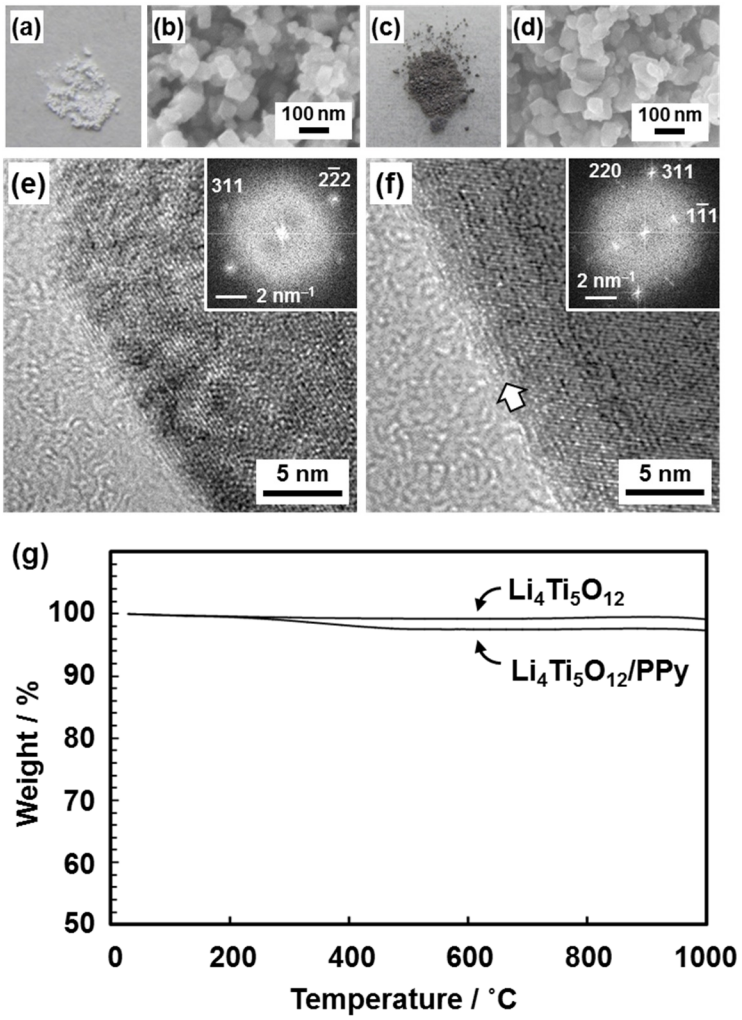

Fig. S10. Conductive coating on $Li_4Ti_5O_{12}$ nanocrystals, an electrode active material for lithium-ion battery. (a–f) macroscopic images (a,c), FESEM images (b,d), and HRTEM images (e,f) of a commercial $Li_4Ti_5O_{12}$ (a,b,e) and the PPy-coated samples (c,d,f). The PPy coating was performed by using $Fe(NO_3)_2 \cdot 9H_2O$ for 3 h. (g) TG curves of the commercial $Li_4Ti_5O_{12}$ and the $Li_4Ti_5O_{12}$/PPy composite.

The powder of commercial $Li_4Ti_5O_{12}$ nanocrystals 20–100 nm in size was set as a substrate with neat liquid of Py and $Fe(NO_3)_2 \cdot 9H_2O$ (Fig. S10a,b). After the coating for 3 h, the color of the powder was changed from white to gray (Fig. S10a,c). The particle sizes were not changed by the coating (Fig. S10b,d). The thin amorphous layer 1 nm in the thickness was partially formed on the nanocrystals (Fig. S10f), while the lattice fringes of the $Li_4Ti_5O_{12}$ were observed throughout the nanocrystals before the PPy coating (Fig. S10e).

It is inferred that the PPy coating is partially achieved on the surface of the $Li_4Ti_5O_{12}$

nanocrystals. Based on the weight loss, the PPy content in the $Li_4Ti_5O_{12}$/PPy composite was estimated to be 1.7 wt.%. The thickness of the PPy coating on the $Li_4Ti_5O_{12}$ nanocrystals is calculated by the following processes. The commercial $Li_4Ti_5O_{12}$ nanocrystals displayed the specific surface area of 32.6 $m^2\ g^{-1}$. Therefore, the average diameter of the nanocrystals are calculated to be 52.6 nm, where the density of $Li_4Ti_5O_{12}$ is 3.50 g cm^{-3}. The 1.7 wt. % of PPy corresponds to the coating 0.35 nm in thickness on the nanocrystals, on the assumption that the density of PPy is 1.50 g cm^{-3}. It is inferred that the thickness is too thin for the coating. The thin amorphous layer was partially observed on the edge of the nanocrystals by FETEM (Fig. S10f). In addition, the coating was started from the PPy nanoparticles on the substrates, as shown in Fig. S3. Therefore, the partial coating of PPy ca. 1 nm in thickness was formed on the $Li_4Ti_5O_{12}$ nanocrystals under the present conditions. The partial coating provides the pathway of both the electron and lithium ion.